

# Hyperbolic and plasmonic properties of Silicon/Ag aligned nanowire arrays

S.M. Prokes,<sup>1\*</sup> Orest J. Glebocki,<sup>1</sup> J. E. Livener,<sup>2</sup> T. U. Tumkur,<sup>2</sup> J. K. Kitur,<sup>2</sup> G. Zhu,<sup>2</sup> B. Wells,<sup>3</sup> V. A. Podolskiy,<sup>3</sup> and M. A. Noginov<sup>2</sup>

<sup>1</sup>Electronic Science and Technology Division, Naval Research Lab, Washington DC, 20375, USA

<sup>2</sup>Center for Materials Research, Norfolk State University, Norfolk, VA 23504, USA

<sup>3</sup>Department of Physics and Applied Physics, University of Massachusetts at Lowell, Lowell, MA, 01854, USA

\*Prokes@nrl.navy.mil

**Abstract:** The hyperbolic and plasmonic properties of silicon nanowire/Ag arrays have been investigated. The aligned nanowire arrays were formed and coated by atomic layer deposition of Ag, which itself is a metamaterial due to its unique mosaic film structure. The theoretical and numerical studies suggest that the fabricated arrays have hyperbolic dispersion in the visible and IR ranges of the spectrum. The theoretical predictions have been indirectly confirmed by polarized reflection spectra, showing reduction of the reflection in p polarization in comparison to that in s polarization. Studies of dye emission on top of Si/Ag nanowire arrays show strong emission quenching and shortening of dye emission kinetics. This behavior is also consistent with the predictions for hyperbolic media. The measured SERS signals were enhanced by almost an order of magnitude for closely packed and aligned nanowires, compared to random nanowire composites. These results agree with electric field simulations of these array structures.

© 2013 Optical Society of America

OCIS Codes: (160.4236) Nanomaterials; (160.3918) Metamaterials; (160.1245) Artificially engineered materials; (160.4670) Optical properties.

---

## References and Links

1. N. Engheta and R. W. Ziolkowski, *Electromagnetic Metamaterials: Physics and Engineering Explorations* (John Wiley & Sons, 2006).
2. M. A. Noginov and V. A. Podolskiy, eds., *Tutorials in Metamaterials*, Series in Nano-optics and Nanophotonics (CRC Press, 2011), p. 293.
3. D. R. Smith, W. J. Padilla, D. C. Vier, S. C. Nemat-Nasser, and S. Schultz, "Composite medium with simultaneously negative permeability and permittivity," *Phys. Rev. Lett.* **84**(18), 4184–4187 (2000).
4. R. A. Shelby, D. R. Smith, and S. Schultz, "Experimental verification of a negative index of refraction," *Science* **292**(5514), 77–79 (2001).
5. A. A. Houck, J. B. Brock, and I. L. Chuang, "Experimental observations of a left-handed material that obeys Snell's law," *Phys. Rev. Lett.* **90**(13), 137401 (2003).
6. C. G. Parazzoli, R. B. Greegor, K. Li, B. E. C. Koltenbah, and M. Tanielian, "Experimental verification and simulation of negative index of refraction using Snell's law," *Phys. Rev. Lett.* **90**(10), 107401 (2003).
7. V. M. Shalaev, W. Cai, U. K. Chettiar, H.-K. Yuan, A. K. Sarychev, V. P. Drachev, and A. V. Kildishev, "Negative index of refraction in optical metamaterials," *Opt. Lett.* **30**(24), 3356–3358 (2005).
8. J. B. Pendry, "Negative refraction makes a perfect lens," *Phys. Rev. Lett.* **85**(18), 3966–3969 (2000).
9. A. Grbic and G. V. Eleftheriades, "Overcoming the diffraction limit with a planar left-handed transmission-line lens," *Phys. Rev. Lett.* **92**(11), 117403 (2004).
10. Z. Jacob, L. V. Alekseyev, and E. Narimanov, "Optical hyperlens: Far-field imaging beyond the diffraction limit," *Opt. Express* **14**(18), 8247–8256 (2006).
11. A. Salandrino and N. Engheta, "Far-field subdiffraction optical microscopy using metamaterial crystals: Theory and simulations," *Phys. Rev. B* **74**(7), 075103 (2006).
12. A. V. Kildishev and E. E. Narimanov, "Impedance-matched hyperlens," *Opt. Lett.* **32**(23), 3432–3434 (2007).
13. I. I. Smolyaninov, Y. J. Hung, and C. C. Davis, "Magnifying superlens in the visible frequency range," *Science* **315**(5819), 1699–1701 (2007).

## Report Documentation Page

*Form Approved*  
*OMB No. 0704-0188*

Public reporting burden for the collection of information is estimated to average 1 hour per response, including the time for reviewing instructions, searching existing data sources, gathering and maintaining the data needed, and completing and reviewing the collection of information. Send comments regarding this burden estimate or any other aspect of this collection of information, including suggestions for reducing this burden, to Washington Headquarters Services, Directorate for Information Operations and Reports, 1215 Jefferson Davis Highway, Suite 1204, Arlington VA 22202-4302. Respondents should be aware that notwithstanding any other provision of law, no person shall be subject to a penalty for failing to comply with a collection of information if it does not display a currently valid OMB control number.

1. REPORT DATE <b>17 JUN 2013</b>	2. REPORT TYPE	3. DATES COVERED <b>00-00-2013 to 00-00-2013</b>	
4. TITLE AND SUBTITLE <b>Hyperbolic and plasmonic properties of Silicon/Ag aligned nanowire arrays</b>		5a. CONTRACT NUMBER	
		5b. GRANT NUMBER	
		5c. PROGRAM ELEMENT NUMBER	
6. AUTHOR(S)		5d. PROJECT NUMBER	
		5e. TASK NUMBER	
		5f. WORK UNIT NUMBER	
7. PERFORMING ORGANIZATION NAME(S) AND ADDRESS(ES) <b>Naval Research Laboratory, Electronic Science and Technology Division, Washington, DC, 20375</b>		8. PERFORMING ORGANIZATION REPORT NUMBER	
9. SPONSORING/MONITORING AGENCY NAME(S) AND ADDRESS(ES)		10. SPONSOR/MONITOR'S ACRONYM(S)	
		11. SPONSOR/MONITOR'S REPORT NUMBER(S)	
12. DISTRIBUTION/AVAILABILITY STATEMENT <b>Approved for public release; distribution unlimited</b>			
13. SUPPLEMENTARY NOTES			
14. ABSTRACT <b>The hyperbolic and plasmonic properties of silicon nanowire/Ag arrays have been investigated. The aligned nanowire arrays were formed and coated by atomic layer deposition of Ag, which itself is a metamaterial due to its unique mosaic film structure. The theoretical and numerical studies suggest that the fabricated arrays have hyperbolic dispersion in the visible and IR ranges of the spectrum. The theoretical predictions have been indirectly confirmed by polarized reflection spectra, showing reduction of the reflection in p polarization in comparison to that in s polarization. Studies of dye emission on top of Si/Ag nanowire arrays show strong emission quenching and shortening of dye emission kinetics. This behavior is also consistent with the predictions for hyperbolic media. The measured SERS signals were enhanced by almost an order of magnitude for closely packed and aligned nanowires, compared to random nanowire composites. These results agree with electric field simulations of these array structures.</b>			
15. SUBJECT TERMS			
16. SECURITY CLASSIFICATION OF:			17. LIMITATION OF ABSTRACT
a. REPORT <b>unclassified</b>	b. ABSTRACT <b>unclassified</b>	c. THIS PAGE <b>unclassified</b>	<b>Same as Report (SAR)</b>
			18. NUMBER OF PAGES <b>13</b>
			19a. NAME OF RESPONSIBLE PERSON

14. Z. W. Liu, H. Lee, Y. Xiong, C. Sun, and X. Zhang, "Far-field optical hyperlens magnifying sub-diffraction-limited objects," *Science* **315**(5819), 1686 (2007).
15. J. B. Pendry, D. Schurig, and D. R. Smith, "Controlling electromagnetic fields," *Science* **312**(5781), 1780–1782 (2006).
16. W. S. Cai, U. K. Chettiar, A. V. Kildishev, and V. M. Shalaev, "Optical cloaking with metamaterials," *Nat. Photonics* **1**(4), 224–227 (2007).
17. D. J. Bergman and M. I. Stockman, "Surface plasmon amplification by stimulated emission of radiation: Quantum generation of coherent surface plasmons in nanosystems," *Phys. Rev. Lett.* **90**(2), 027402 (2003).
18. M. T. Hill, Y.-S. Oei, B. Smalbrugge, Y. Zhu, T. De Vries, P. J. Van Veldhoven, F. W. M. Van Otten, T. J. Eijkeman, J. P. Turkiewicz, H. De Waardt, E. J. Geluk, S.-H. Kwon, Y.-H. Lee, R. N. Tzel, and M. K. Smit, "Lasing in metallic-coated nanocavities," *Nat. Photonics* **1**(10), 589–594 (2007).
19. M. A. Noginov, G. Zhu, A. M. Belgrave, R. Bakker, V. M. Shalaev, E. E. Narimanov, S. Stout, E. Herz, T. Suteewong, and U. Wiesner, "Demonstration of a spaser-based nanolaser," *Nature* **460**(7259), 1110–1112 (2009).
20. R. F. Oulton, V. J. Sorger, T. Zentgraf, R.-M. Ma, C. Gladden, L. Dai, G. Bartal, and X. Zhang, "Plasmon lasers at deep subwavelength scale," *Nature* **461**(7264), 629–632 (2009).
21. M. Khajavikhan, A. Simic, M. Katz, J. H. Lee, B. Slutsky, A. Mizrahi, V. Lomakin, and Y. Fainman, "Thresholdless nanoscale coaxial lasers," *Nature* **482**(7384), 204–207 (2012).
22. D. R. Smith and D. Schurig, "Electromagnetic wave propagation in media with indefinite permittivity and permeability tensors," *Phys. Rev. Lett.* **90**(7), 077405 (2003).
23. P. A. Belov, R. Marqués, S. I. Maslovski, I. S. Nefedov, M. Silveirinha, C. R. Simovski, and S. A. Tretyakov, "Strong spatial dispersion in wire media in the very large wavelength limit," *Phys. Rev. B* **67**(11), 113103 (2003).
24. Z. Jacob, L. V. Alekseyev, and E. Narimanov, "Optical Hyperlens: Far-field imaging beyond the diffraction limit," *Opt. Express* **14**(18), 8247–8256 (2006).
25. A. Salandrino and N. Engheta, "Far-field subdiffraction optical microscopy using metamaterial crystals: Theory and simulations," *Phys. Rev. B* **74**(7), 075103 (2006) (5 pages).
26. Z. Jacob, I. I. Smolyaninov, and E. E. Narimanov, "Broadband Purcell effect: Radiative decay engineering with metamaterials," *Appl. Phys. Lett.* **100**(18), 181105 (2012).
27. M. A. Noginov, H. Li, Y. A. Barnakov, D. Dryden, G. Nataraj, G. Zhu, C. E. Bonner, M. Mayy, Z. Jacob, and E. E. Narimanov, "Controlling spontaneous emission with metamaterials," *Opt. Lett.* **35**(11), 1863–1865 (2010).
28. H. N. S. Krishnamoorthy, Z. Jacob, E. Narimanov, I. Kretzschmar, and V. M. Menon, "Metamaterial based broadband engineering of quantum dot spontaneous emission," arXiv:0912.2454.
29. Z. Jacob, J.-Y. Kim, G. V. Naik, A. Boltasseva, E. E. Narimanov, and V. M. Shalaev, "Engineering photonic density of states using metamaterials," *Appl. Phys. B* **100**(1), 215–218 (2010).
30. T. Tumkur, G. Zhu, P. Black, Yu. A. Barnakov, C. E. Bonner, and M. A. Noginov, "Control of spontaneous emission in a volume of functionalized hyperbolic metamaterial," *Appl. Phys. Lett.* **99**(15), 151115 (2011).
31. J. Kim, V. P. Drachev, Z. Jacob, G. V. Naik, A. Boltasseva, E. E. Narimanov, and V. M. Shalaev, "Improving the radiative decay rate for dye molecules with hyperbolic metamaterials," *Opt. Express* **20**(7), 8100–8116 (2012).
32. H. N. S. Krishnamoorthy, Z. Jacob, E. Narimanov, I. Kretzschmar, and V. M. Menon, "Topological transitions in metamaterials," *Science* **336**(6078), 205–209 (2012).
33. A. N. Poddubny, P. A. Belov, and Y. S. Kivshar, "Spontaneous radiation of a finite-size dipole emitter in hyperbolic media," *Phys. Rev. A* **84**(2), 023807 (2011).
34. E. M. Purcell, "Spontaneous emission probabilities at radio frequencies," *Phys. Rev.* **69**, 681 (1946).
35. T. U. Tumkur, J. K. Kitur, B. Chu, L. Gu, V. A. Podolskiy, E. E. Narimanov, and M. A. Noginov, "Control of reflectance and transmittance in scattering and curvilinear hyperbolic metamaterials," *Appl. Phys. Lett.* **101**(9), 091105 (2012).
36. E. E. Narimanov, H. Li, Yu. A. Barnakov, T. U. Tumkur, and M. A. Noginov, "Reduced reflection from roughened hyperbolic metamaterial," submitted to *Optics Express*.
37. A. Boltasseva, "Fabrication of optical metamaterials," in *Tutorials in Metamaterials*, (Series in Nano-optics and Nanophotonics) A. M. A. Noginov and V. A. Podolskiy, Eds. (CRC Press, 2011).
38. P. R. Evans, G. A. Wurtz, R. Atkinson, W. Hendren, D. O'Connor, W. Dickson, R. J. Pollard, and A. V. Zayats, "Plasmonic core/shell nanorod arrays: subattoliter controlled geometry and tunable optical properties," *J. Phys. Chem. C* **111**(34), 12522–12527 (2007).
39. W. Dickson, G. A. Wurtz, P. Evans, D. O'Connor, R. Atkinson, R. Pollard, and A. V. Zayats, "Dielectric-loaded plasmonic nanoantenna arrays: A metamaterial with tuneable optical properties," *Phys. Review B* **76** 115411 (2007).
40. A. V. Kabashin, P. Evans, S. Pastkovsky, W. Hendren, G. A. Wurtz, R. Atkinson, R. Pollard, V. A. Podolskiy, and A. V. Zayats, "Plasmonic nanorod metamaterials for biosensing," *Nat. Mater.* **8**(11), 867–871 (2009).
41. J. Yao, Z. Liu, Y. Liu, Y. Wang, C. Sun, G. Bartal, A. M. Stacy, and X. Zhang, "Optical negative refraction in bulk metamaterials of nanowires," *Science* **321**(5891), 930 (2008).
42. M. A. Noginov, Yu. A. Barnakov, G. Zhu, T. Tumkur, H. Li, and E. E. Narimanov, "Bulk photonic metamaterial with hyperbolic dispersion," *Appl. Phys. Lett.* **94**(15), 151105 (2009).
43. D. A. Pawlak, "Eutectic fibers with self-organized structures," *Adv. Mater. Res.* **8**, 129–139 (2007).

44. A. J. Hoffman, L. Alekseyev, S. S. Howard, K. J. Franz, D. Wasserman, V. A. Podolskiy, E. E. Narimanov, D. L. Sivco, and C. Gmachl, "Negative refraction in semiconductor metamaterials," *Nat. Mater.* **6**(12), 946–950 (2007).
45. S. M. Prokes, O. J. Glembocki, E. Cleveland, J. D. Caldwell, E. Foos, J. Niinistö, and M. Ritala, "Spoof-like plasmonic behavior of plasma enhanced atomic layer deposition grown Ag thin films," *Appl. Phys. Lett.* **100**(5), 053106 (2012).
46. Y. Wu, Y. Cui, L. Huynh, C. J. Barrelet, D. C. Bell, and C. M. Lieber, "Controlled growth and structures of molecular-scale silicon nanowires," *Nano Lett.* **4**(3), 433–436 (2004).
47. H. Pan, S. Lim, C. Poh, H. Sun, X. Wu, Y. Feng, and J. Lin, "Growth of Si nanowires by thermal evaporation," *Nanotechnology* **16**(4), 417–421 (2005).
48. J. Westwater, D. Gosain, S. Tomiya, and S. Usui, "Growth of silicon nanowires via gold/silane vapor-liquid-solid reaction," *J. Vac. Sci. Technol. B* **15**(3), 554 (1997).
49. K. Peng, Y. J. Yan, S. P. Gao, and J. Zhu, "Synthesis of large-area silicon nanowire arrays via self-assembling nanoelectrochemistry," *Adv. Mater.* **14**(16), 1164 (2002).
50. M. L. Zhang, K. Peng, X. Fan, J. S. Jie, R. Q. Zhang, S. T. Lee, and N. B. Wong, "Preparation of large/area uniform silicon nanowires arrays through metal-assisted chemical etching," *J. Phys. Chem. C* **112**(12), 4444–4450 (2008).
51. M. Kariniemi, J. Niinistö, T. Hatanpää, M. Kemell, T. Sajavaara, M. Ritala, and M. Leskela, "Plasma-enhanced atomic layer deposition of silver thin films," *Chem. Mater.* **23**(11), 2901–2907 (2011).
52. O. J. Glembocki, S. M. Prokes, E. Cleveland, R. W. Rendell, and E. Foos, "Metamaterial properties of silver films deposited by ALD," *Proceeding of ALD 2012*, **129** (2012).
53. [www.comsol.com](http://www.comsol.com)
54. *Handbook of Optical Constants of Solids*, E. D. Palik, ed. (Academic, 1998)
55. R. J. Pollard, A. Murphy, W. R. Hendren, P. R. Evans, R. Atkinson, G. A. Wurtz, A. V. Zayats, and V. A. Podolskiy, "Optical nonlocalities and additional waves in epsilon-near-zero metamaterials," *Phys. Rev. Lett.* **102**(12), 127405 (2009).
56. N. Felidj, J. Aubard, G. Levi, J. R. Krenn, A. Hohenau, G. Schider, A. Leitner, and F. R. Assenegg, "Optimized surface-enhanced Raman scattering on gold nanoparticle arrays," *Appl. Phys. Lett.* **82**(18), 3095 (2003).
57. S. M. Prokes, O. J. Glembocki, R. W. Rendell, and M. G. Ancona, "Enhanced plasmon coupling in crossed dielectric/metal nanowire composite geometries and applications to surface-enhanced Raman spectroscopy," *Appl. Phys. Lett.* **90**(9), 093105 (2007).
58. S. M. Prokes, D. A. Alexson, O. J. Glembocki, H. D. Park, and R. W. Rendell, "Effect of crossing geometry on the plasmonic behavior of dielectric core/metal sheath nanowires," *Appl. Phys. Lett.* **94**(9), 093105 (2009).
59. R. Aroca and A. Thedchanamoorthy, "Vibrational studies of molecular organization in evaporated phthalocyanine thin solid films," *Chem. Mater.* **7**(1), 69–74 (1995).
60. M. Lütt, M. R. Fitzsimmons, and D. Li, "X-ray reflectivity study of self-assembled thin films of macrocycles and macromolecules," *J. Phys. Chem. B* **102**(2), 400–405 (1998).
61. J. P. Kottmann and O. J. F. Martin, "Plasmon resonant coupling in metallic nanowires," *Opt. Express* **8**(12), 655–663 (2001).

---

## 1. Introduction

*Metamaterials* are engineered composite materials containing subwavelength inclusions with rationally designed shapes, sizes, mutual arrangements and orientations, which often exhibit unparalleled properties not available in nature or traditional synthetic materials [1,2]. The field of metamaterials has brought about novel designs, since researchers have been able to overcome the constraints associated with conventional materials and explore entirely new concepts with a much larger range of material parameters available through structured media. Materials with negative indices of refraction [3–7], "perfect" lenses [8,9] and hyperlenses [10–14] that focus and image with resolution beyond the diffraction limit, invisibility cloaks [15,16], and nanoscopic lasers [17–21] are just some of the novel concepts that have been put forward.

A new class of uniaxial (meta)materials has been reported [22–25], which have highly unusual iso-frequency surfaces defined by allowed wavevectors at constant frequency. When all principal components of the dielectric permittivity tensor are positive, the iso-frequency surface is "closed" and forms a spheroid or ellipsoid in the wavevector space ( $k$ -space). In such media, the magnitude of the wavenumber is limited, constraining the resolution of optical imaging, and the density of photonic states. In contrast, a highly anisotropic metamaterial, whose dielectric permittivity in orthogonal directions has different signs, exhibits a hyperbolic iso-frequency surface, and thus is referred to as hyperbolic. Such materials have an almost unlimited magnitude of a wave vector  $k$  and near infinite local

density of photonic states [26]. Recent theoretical predictions [26] and experimental results in hyperbolic metamaterial structures [27–33] have shown that, in line with the seminal work by Purcell [34], the high density of photonic states can control spontaneous emission of luminescent centers and reflectance of roughened metamaterials' surfaces [35,36].

The most common approach to fabricate a metamaterial is by patterning periodic arrays of individual elements, which can be metal, dielectric, plastics, etc., depending on application. The properties of metamaterials can then be tailored by controlling the individual element shape, size and geometry, as well as the array periodicity and/or arrangement [1,2]. However, most of traditional cleanroom fabrication techniques are prohibitively expensive and hardly scalable [37]. Much more appealing are bottom-up techniques capable of producing centimeter size samples, which include electroplating growth of metallic nanowires in porous alumina membranes [38–42], eutectic crystal growth of split ring resonator structures [43], and deposition of lamellar semiconductor or metal-dielectric film structures [28–32,44]. In addition, a metamaterial can also be formed by Atomic Layer Deposition (ALD) growth-induced patterning, as has recently been reported for Ag [45].

The density of photonic states in hyperbolic metamaterials (which can control a variety of quantum and classical phenomena) is significantly larger *inside* the structure than on its surface [29]. Therefore, many applications require impregnation of hyperbolic metamaterials with nonlinear and luminescent chromophores and other active components. One realization of hyperbolic metamaterials, allowing their easy functionalization, is arrays of parallel metal-coated nanowires that are separated by air gaps, which is studied in this work theoretically and experimentally.

In this work, we fabricate and examine the optical properties of closely spaced long Si/Ag nanowire composite arrays. We predict, theoretically and numerically, that these structures have hyperbolic dispersion in the visible and infrared ranges of the spectrum. The results of reflection and dye emission experiments are consistent with the model predictions. We also report an enhancement of surface enhanced Raman scattering (SERS), which is, most likely, due to plasmonic coupling of closely spaced nanowires and enhanced density of photonic states in hyperbolic metamaterials.

## 2. Formation of closely spaced Si nanowire arrays

There are a number of approaches in forming silicon nanowires (NWs), such as chemical vapor deposition [46] and thermal evaporation [47], but in general, these processes require very specific growth chambers which are expensive and which can require rather dangerous gases, such as silane. Furthermore, most of these systems produce randomly grown Si nanowires. In order to form aligned and ordered Si nanowire arrays with small diameters, the vapor liquid solid (VLS) growth mechanism is used [48], and small diameter nanowires can be formed by control of the metal catalyst size, which may require further lithographic steps. Instead, we have chosen a metal assisted chemical etching process [49], which allows a simple and inexpensive way of forming silicon nanowire arrays, with very few equipment requirements.

Preparation of silicon nanowires through chemical etching has been found to work well when silver is used to enhance the etching [50]. The etching process can be described as follows: Ag nanoparticles are deposited onto the silicon substrate. Some of the Ag is oxidized and dissolved in solution, forming Ag<sup>+</sup> ions, which react with Si at the Si/Ag nanoparticle interface, so that enhanced silicon etching occurs, and it is localized to the regions covered by the Ag nanoparticles. As this enhanced Si etching continues, channels are formed into the silicon substrate, leaving silicon walls in regions with no Ag nanoparticles, thus creating a Si NW array.

A number of Silicon substrates were investigated, including Si(100), Si(111), lightly doped p and n-type wafers, heavily doped p and n-type wafers, as well as p-doped 50 micron thick Si wafers. The silicon wafers were cut into 1x1 cm<sup>2</sup> pieces, washed with acetone,

ethanol, and DI water, followed by a piranha etch (sulfuric acid and hydrogen peroxide in a 3:1 v/v ratio). The samples were then dipped in 5% HF/water solution for 3 minutes, placed in a 4.8 M HF and 0.005M AgNO<sub>3</sub> solution to form the Ag catalyst [49]. The resultant samples were rinsed in deionized (DI) water and the remaining Ag catalyst was removed using a nitric acid/DI solution. The nanowires were characterized via scanning electron microscopy (SEM).

### 2.1 Effect of Si substrate doping on array formation

A number of silicon substrates were investigated, using the optimal electroless Ag catalyst deposition and optimal HF etching conditions. Figure 1 shows the SEM images of some of the resulting nanowires etched under the same conditions as a function of substrate doping. Figure 1(a) shows an SEM micrograph of a lightly boron doped p-type silicon wafer with a resistivity of 1-30 ohm-cm, Fig. 1(b) shows an image for a lightly phosphorus doped n-type silicon with a resistivity of 1-20 ohm-cm, Fig. 1(c) shows a heavily boron doped p-type silicon wafers with resistivity of 0.01-0.02 ohm-cm, Fig. 1(d) shows a heavily arsenic doped n-type silicon with a resistivity of 0.0015-0.007 ohm-cm and Fig. 1(e) shows Si arrays that can be formed on both sides of a Si wafer, assuming the etching conditions are properly optimized.

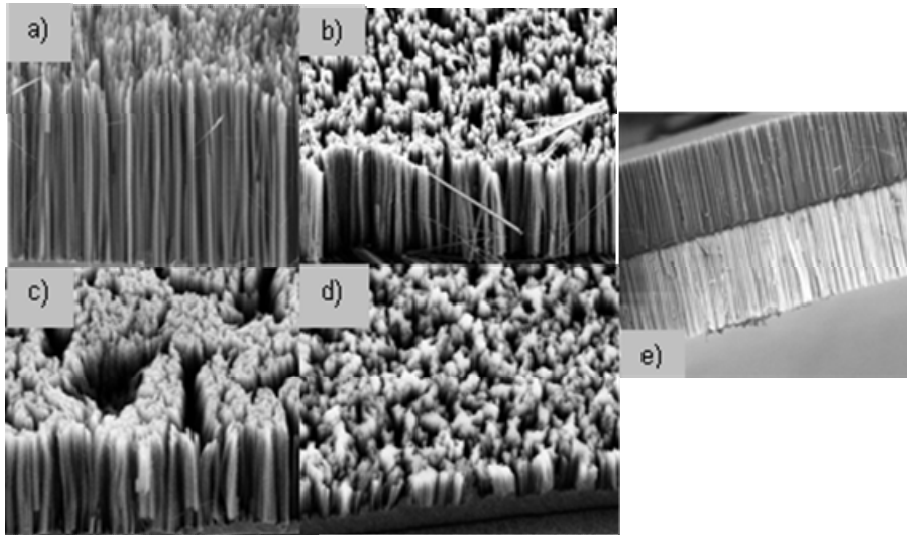


Fig. 1. Si NWs produced using a) p-type silicon, 1-30 ohm-cm, b) n-type silicon, 1-20 ohm-cm, c) p-type silicon, 0.01-0.02 ohm-cm, d) n-type silicon, 0.0015-0.007 ohm-cm and e) p-type Si (100) 50 micron thick wafer, etched from both sides.

As is evident from Fig. 1, the metal assisted chemical etching process worked well for most types of silicon substrates except those that were heavily doped. This is evident in Fig. 1(d) for a very heavily doped sample, which resulted in short, disordered nanowires that were not properly separated from each other.

### 3. Formation of NW/Ag composite arrays

In order to investigate both hyperbolic and plasmonic properties of the NW arrays, we coated the Si NW arrays with 21 nm of Ag, using atomic layer deposition (ALD). The ALD process, due to its conformality and high aspect ratio coverage, was deemed ideal for achieving full coverage of the closely spaced NW arrays.

The growth of the Ag films was performed by remote plasma enhanced atomic layer deposition (PEALD), using Ag(fod)(PET<sub>3</sub>) (fod = 2,2-dimethyl-6,6,7,7,8,8,8-

heptafluorooctate-3,5-dionato) and hydrogen plasma as the precursors [45, 51]. The Ag films were deposited at 125°C onto the Si nanowire arrays, as well as on random Si nanowires.

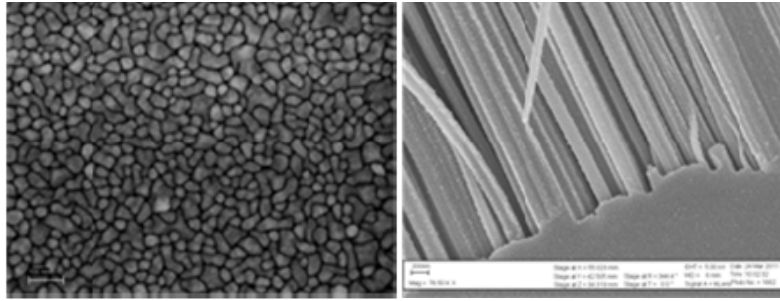


Fig. 2. a) SEM image of 21 nm thick Ag thin film deposited on Si using plasma enhanced atomic layer deposition (PEALD); b) SEM image of Si NW arrays coated with ALD Ag near the substrate.

The thicknesses of the deposited Ag films were 7 nm, 17 nm, 21 nm and 38 nm, as measured by ellipsometry and XTEM.

The PEALD film consisted of polycrystalline fcc flat Ag islands (Fig. 2(a)), separated by very small air gaps. No detectable contaminants (from EDS) were noted and the thicker films had a resistivity in line with metallic Ag. In terms of coating the Si NW arrays, although the Si nanowires in the arrays were 30 microns long and relatively closely spaced (separated by only 150 - 200 nm), we see conformal coverage of the ALD Ag along the whole length, down to the substrate, as shown in Fig. 2(b).

In terms of the optical response, however, the ALD Ag does not resemble a standard Ag thin film, in that the ALD Ag exhibits plasmonic behavior, as reported earlier [45]. This plasmonic behavior is also evident from Fig. 3(a), which shows an experimentally determined reflection spectrum for the PEALD Ag, along with an FDTD simulation of this Ag mosaic structure. The resonance near 600 nm is due to plasmonics, and it has been shown to blue shift with decreasing film thickness [52]. This resonance is only present in ALD Ag and not in Ag films deposited by other means [52], which agrees well with the SERS enhancement only seen for ALD Ag [45]. Thus PEALD Ag is in fact a metamaterial due to its unique mosaic grain structure, modeled as a coaxial cylinder of Ag surrounded by an air gap [45]. Figure 3(b) shows a single coaxial cylinder used to model the Ag ALD film mosaic morphology in the FDTD simulation. The simulation was obtained by forming an array of these cylinders

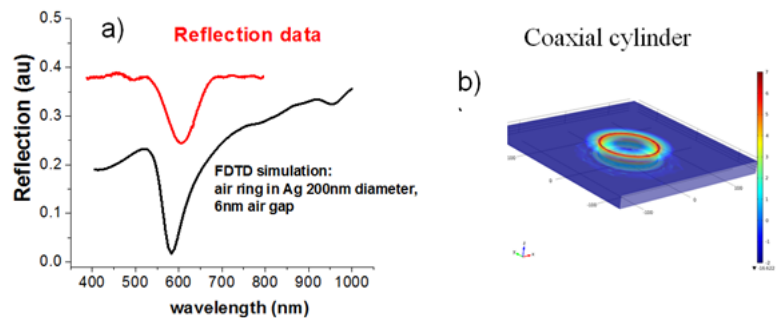


Fig. 3. a) Comparison of the measured reflection data of ALD Ag to a finite difference time domain simulation of a 200nm diameter air ring in a 40nm thick Ag film. Note that the data and simulation both have the same line shape and that the positions of the resonance agree well. b) Electric field simulation of a single element of the PEALD Ag microstructure (coaxial cylinder) used to obtain the simulation in a). Also shown are the resultant high electric fields in and above the air gap.

in order to obtain the reflection data shown in Fig. 3(a) and the electric field enhancements shown in red in Fig. 3(b). Note that these high electric fields form not only in the air gaps but also above the gaps, which leads to strong plasmonic behavior as measured by SERS [45].

#### 4. Theoretical prediction of Hyperbolic Dispersion

To understand the topological properties of the waves propagating in our metamaterials, we used 2D finite-element-based solutions of Maxwell equations [53] to deduce the dependence of the z-component of wavevector on frequency and x-component of the wavevector. In these calculations we used a more general model of the structure than the one realized in experiments. Thus, the system was represented as a periodic array of infinitely long composite wires with shelled internal structure (one unit cell of such structure is shown in Fig. 4(a)). These calculations have revealed that, similar to previously studied nanowire-based metamaterials [38–42], Si-based nanowire arrays support two waves that differ by their polarization. The dispersion of these two waves was numerically calculated for the following set of parameters: free-space wavelength 900 nm, distance between centers of Si nanowires 250 nm, the diameter of nanowires: 150 nm, with thickness of ALD silver coatings ranging from 7 nm to 38 nm. In these calculations, we assumed that optical properties of components of metamaterials are significantly close to those of bulk media [54].

The calculations show that for small angles of incidence, the behavior of the metamaterial is consistent with what is expected of a uniaxial homogeneous medium. For smaller values of silver thickness, the material exhibits elliptical behavior, while for larger thickness of the silver shells, the behavior is hyperbolic-like. Least-square fitting of these numerically calculated dispersion curves to ellipses or hyperbolae yields the effective medium parameters for the structure [40]. These effective medium parameters are summarized in Fig. 4(b).

In the limit when the nanowire radius, shell thickness, and distance between the wires are much smaller than the wavelength, the dispersion of nanowire structures can be described by

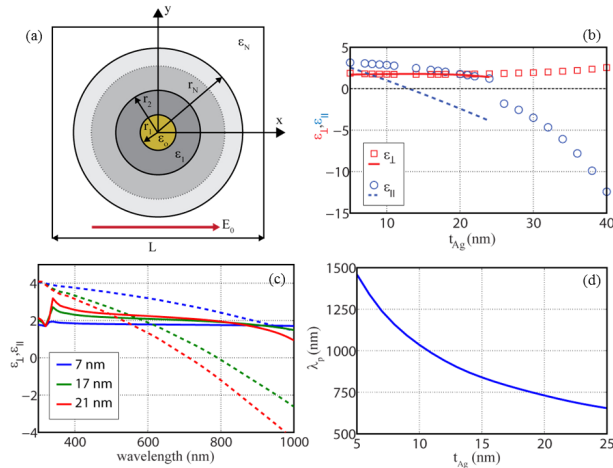


Fig. 4. (a) schematic geometry of the unit cell for a multi-shell nanowire composite, used in derivation of effective medium response; experimental configuration corresponds to a two shell system or  $N = 2$ ; (b) effective medium parameters extracted from finite-element solutions of Maxwell equations (symbols) and from effective medium theory (lines); (c) spectral dependence of effective medium parameters for different thickness of Ag shell; (d) dependence of effective plasma wavelength of composite in (c) as a function of Ag shell thickness.

effective medium theory that can be calculated by straightforward generalization of Maxwell-Garnett approach to describe the composite containing  $N$  shell-type components. Explicitly, the component of the permittivity tensor along the wire,  $\epsilon_{zz}$ , is calculated as the weighed average of the permittivities of the constituent components as

$$\varepsilon_{\parallel} = \varepsilon_{zz} = \sum_i p_i \varepsilon_i, \quad (1)$$

with  $p_i$  being the (surface) concentration of the  $i$ -th component of the composite.

To calculate the component of permittivity tensor in the direction perpendicular to the wires, it is necessary to find field distribution along the nanowire system. Straightforward calculation yields:

$$\varepsilon_{\perp} = \varepsilon_{xx} = \varepsilon_{yy} = \sum_i \frac{p_i \varepsilon_i e_i}{p_i e_i} \quad (2)$$

with parameters  $e_i$  calculated using a simple iterative technique:

$$\begin{aligned} e_{i-1} &= T_i e_i \\ T_i &= \frac{2}{\frac{\varepsilon_{i-1}}{\varepsilon_i} \left(1 - \frac{S_{i-1}}{r_i^2}\right) + \left(1 + \frac{S_{i-1}}{r_i^2}\right)} \\ S_i &= r_i^2 \left[ \left(1 + \frac{S_{i-1}}{r_i^2}\right) T_i - 1 \right] \\ S_0 &= 0, e_N = 1 \end{aligned} \quad (3)$$

The agreement of the numerically-extracted effective medium parameters with prediction of generalized Maxwell-Garnett theory is illustrated in Fig. 4(b). It is seen that the iterative technique adequately describes the behavior of  $\varepsilon_{\perp}$  in the regime when the concentration of inclusions is relatively small (the relative concentration of the host component of metamaterial  $p_N > 70\%$ ). In contrast, the parallel component of the permittivity is only qualitatively described by the effective medium theory. This apparent disagreement has its origin in strong spatial dispersion that is expected in the vicinity of epsilon-near-zero behavior for composites with relatively large unit cells. Similar deviations have been previously observed in gold nanowire metamaterials [55]. The implications of this behavior for optical response of the nanowire composites and the analytical description of the properties of nanowire systems in ENZ regime will be detailed in our future works.

To explore the parameter space enabled by the Si/Ag nanowire arrays, effective medium theory was used to analyze the dependence of effective medium parameters as a function of wavelength for several fixed values of the Ag shell thickness. The results of these calculations are summarized in Fig. 4(c). It is seen that, similar to conventional plasmonic nanowire arrays, Si/Ag composites offer broadband hyperbolic response, with plasma-like behavior of  $\varepsilon_{\parallel}$ . As expected, the thickness of plasmonic shell plays a role of a convenient control parameter, that can be used to tune effective plasma frequency (the frequency at which  $\varepsilon_{\parallel}$  crosses zero). Such tuning is shown in Fig. 4(d).

## 5. Experimental Studies of Reflection and Emission in Si/Ag arrays

### 5.1 Specular and Diffused Reflection of Si/Ag arrays

The four nanowire samples with the parameters described in Section 4 and thickness of ALD silver equal to 7 nm, 17 nm, 21 nm and 38 nm have been studied experimentally. According to the theoretical modeling presented in Section 4, all these samples have hyperbolic dispersion in the red and infrared ranges of the spectrum. All of them looked dark gray, likely due to a combination of roughness, which is inherent to nanomaterials fabricated by etching, and (as explained below) preferential scattering of light *inside* roughened hyperbolic metamaterials [35, 36]. Correspondingly, the specular reflection of the samples was very low, under 0.5%. We have attempted to obtain the values of dielectric permittivities extracted from

the angular reflectance data (following [42]). However, due to the very weak specular reflection and strong diffused scattering, it is not clear if meaningful results can be obtained by this method.

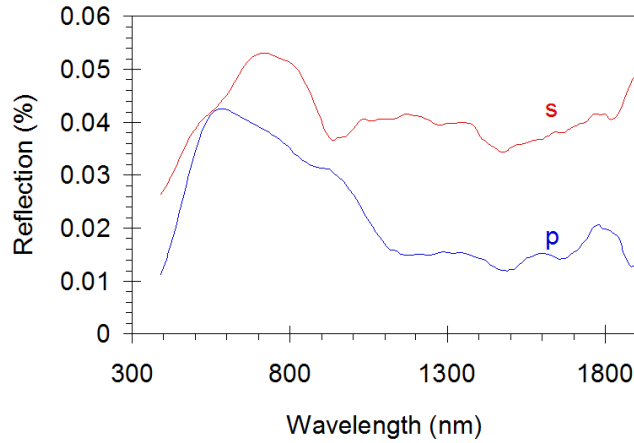


Fig. 5. Reflection spectra of Si/ALD silver sample with 21 nm ALD silver coating, measured in p and s polarizations in an integrating sphere setup at  $\sim 10^\circ$  incidence angle.

At the same time, the reflection measured in an integrated sphere setup (which captured both specularly reflected light and diffusely reflected light) was significantly larger; see for example Fig. 5, depicting the reflection spectrum of the sample with 21 nm ALD silver coating. One can see that the reflectivity in p polarization is significantly smaller than that in s polarization, in particular in the near-infrared part of the spectrum. This is expected from rough surfaces of metamaterials with hyperbolic dispersion [35,36], in which enhanced scattering of p polarized light *inside* the hyperbolic medium (where the density of photonic states is high) causes substantial reduction of reflection. No substantial reduction of reflectance is predicted for s polarized light [36]. Correspondingly, the experimental result depicted in Fig. 5 is consistent with the theoretical prediction of hyperbolic dispersion in the sample.

### 5.2 Kinetics and intensity of dye emission on top of Si/Ag nanowire array

In this particular experiment, we studied the array of Si/Ag nanowires coated with 21 nm ALD silver layer. A film of polymethyl methacrylate (PMMA) doped with IR140 laser dye (in concentration 0.013 M) was deposited on top of the nanowire array sample and onto the control substrates, which were glass and silver film deposited on glass. The film thickness in control samples was  $\sim 80$  nm. The Si/Ag nanowire sample had approximately the same concentration of dye molecules per unit area of the sample. However, dye penetrated in the voids between nanowires, and the effective thickness could not be determined.

In order to measure the emission kinetics, the IR140:PMMA films were pumped using a 100 fs Ti:sapphire laser at  $\lambda = 792$  nm. The emission was detected using a near-infrared Hamamatsu streak camera equipped with appropriate long-pass filters ( $\lambda > 850$  nm). All emission kinetics, averaged over multiple measurements, along with the kinetics of the pumping pulse scattered by a pure glass substrate (which shows the time resolution of the apparatus determined by jitter of the laser and wide open slit of the streak camera) are depicted in Fig. 6. One can see that the emission of dye on top of the metamaterial sample is strongly quenched in first  $\sim 100$  ps, and its decay kinetics is significantly shortened (more than twofold in comparison to the control samples) at longer times.

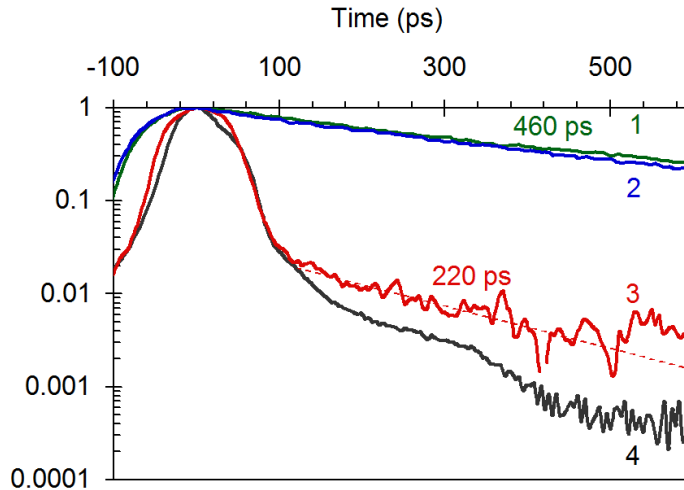


Fig. 6. (a) Spontaneous emission kinetics of the IR140:PMMA film deposited on the top of glass (1), 200 nm thick silver film (2), and the Si/ALD Ag metamaterial sample (3). Trace 4 shows the time resolution of the apparatus.

We have also studied the emission spectra of IR140:PMMA films deposited on top of the metamaterial sample and the glass substrate. In this particular experiment, the samples were pumped at 784 nm. The emission signal was detected with a photomultiplier tube (PMT) connected to the exit slit of a monochromator. The emission spectra are shown in Fig. 7. It can be seen that the emission of IR140:PMMA deposited on top of the metamaterial, is almost one order of magnitude smaller compared to the same dye-doped film deposited on glass. (The difference can be even larger considering the large error bar.)

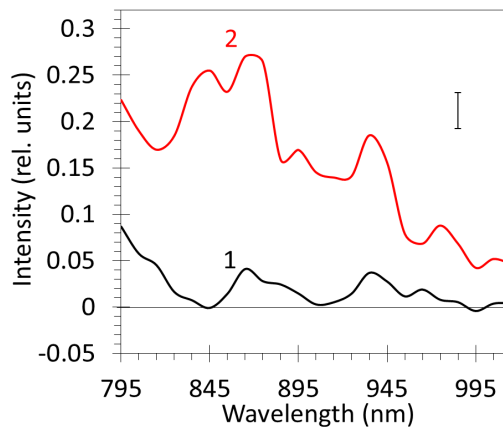


Fig. 7. Spontaneous emission spectra of the IR140:PMMA film deposited on top of the Si/Ag metamaterial sample with 21 nm ALD silver coating (1) and glass (2), pumped at  $\lambda = 784$  nm into the absorption band of IR140.

The experimentally observed reduction of the dye emission intensity and shortening of the emission kinetics are consistent with the theoretical predictions for hyperbolic metamaterials [26]. In fact, high density of photonic states on the surface (and inside) of a metamaterial with hyperbolic dispersion causes enhancement of spontaneous emission directed *inside* the material. This determines the emission kinetics shortening and reduction of the emission

intensity. Similar emission quenching and shortening of the emission decay time have been observed in a dye-doped film deposited on top of array of silver nanowires grown in alumina membrane [27].

### 5.3 Angular distribution of dye emission in Si/Ag nanowire array

Hyperbolic metamaterials have been predicted to produce cone-shaped or beam-like patterns of spontaneous emission inside the medium [26]. The angular distribution of emission outside the sample is much less researched. In the experimental study of this phenomenon, we deposited PMMA film doped with HITC laser dye (in concentration 0.04 M) onto array of Si/Ag nanowires with 38 nm silver coating as well as onto ALD silver film and thermal vapor deposited silver film. The thickness of the dye-doped PMMA films on top of silver films was ~80 nm. In the Si/Ag nanowire sample, dye (which had approximately the same concentration of dye molecules per unit area) penetrated between the wires.

Dye molecules were excited with ~5 ns pulses of the optical parametric oscillator (OPO) at  $\lambda = 750$  nm and  $45^\circ$  incidence angle. The emission intensity was measured, in the spectral band centered at 815 nm, at a variety of detection angles ranging from  $0^\circ$  (normal to the sample surface) to  $\sim 90^\circ$  (parallel to the surface). A long-pass filter in front of the detector blocked laser pumping and transmitted dye emission.

Angular distributions of emission in three samples studied are depicted in Fig. 8. One can see that the emission patterns from the Si/Ag nanowire array and ALD silver film are very close to Lambertian ( $\sim \cos(\theta)$ ). This behavior could probably be expected, since surfaces of both samples are rough (the roughness of Si/Ag NW array much larger than that of ALD silver.) At the same time, the emission of dye on top of a much smoother ( $>5$ nm) thermal vapor deposited silver is slightly broader. The comparison of the experiment with the theory will be published elsewhere.

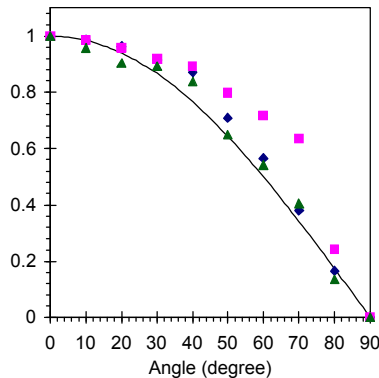


Fig. 8. Angular distributions of emission of HITC dye molecules on top of Si/Ag NW array (diamonds), ALD silver film (triangles) and silver film deposited via thermal vapor deposition (squares). Solid line:  $\cos(\theta)$ .

## 6. Plasmonic Properties of Nanowire Arrays

Raman scattering is a technique, which can measure interatomic vibrations that are unique to each material, thus providing a chemical “fingerprint” for any material. Unfortunately, the scattering efficiencies are very low, roughly  $10^{-8}$  of the incident laser light. However, the signal can be greatly enhanced by the use of metal nanoparticles, which enhance the local electric fields [56]. This process is referred to as Surface Enhanced Raman Scattering (SERS). One type of SERS nanostructures resulting in strong SERS signal are dielectric core/metal sheath nanowires [57,58], which have been shown to create electric field hotspots

at their crossings due to plasmonic coupling. It has also been shown that two closely spaced parallel dielectric core/metal sheath nanowires result in a greater enhancement than those crossed at  $90^\circ$  [58].

A self-assembled monolayer of benzenethiol (BZT) was deposited on the NW arrays by soaking them in  $10^{-4}$  M BZT/toluene solution overnight and rinsing with methanol, which removed excess BZT not bonded to the Ag surface. The SERS spectra were obtained using a DeltaNu Reporter 785 micro-Raman system, operating at 785 nm and the spectra were collected with a laser power of less than 3 mW. In addition, COMSOL electric field calculations were performed in order to interpret the experimental SERS results. The SERS results for the Si/Ag NW arrays are shown in Fig. 9(a). The major Raman peaks can be assigned to symmetric ring breathing, in plane C–H bending and in plane C–C stretching of the phenyl ring from the active molecules, benzenethiol (BT), which are in good agreement with those reported previously [59, 60]. As can be seen, very strong lines associated with the BZT molecule are seen, and the uniformity of the SERS signal intensity is quite uniform

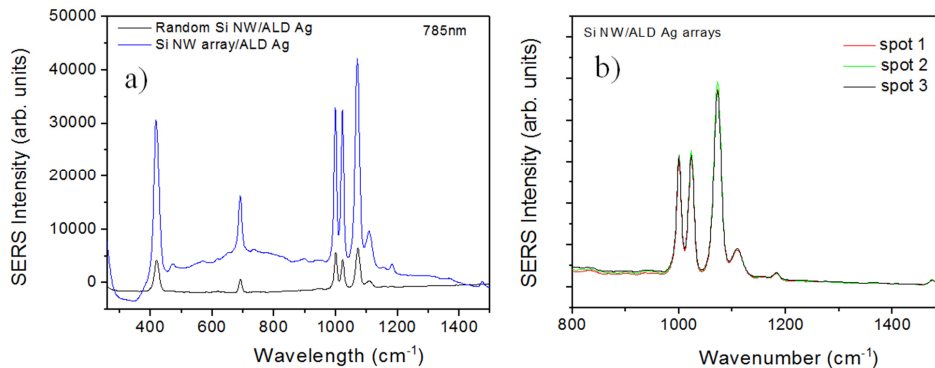


Fig. 9. (a) SERS spectrum for benzenethiol (BZT) for Si/Ag NW arrays compared to horizontal random Si/Ag NWs, and (b) SERS spectrum for three random locations on the Si NW array.

when taken from different regions of the sample (Fig. 9(b)). More importantly, the SERS signal of the closely spaced Si/Ag NW arrays is a factor of 7 stronger compared to a similar density of random Si/Ag nanowires placed on a flat Si substrate, Fig. 9(a). To arrive at this number, the SERS intensity of the arrays was normalized to the total number of NWs in a 2 micron diameter area (laser spot size). Similarly, the SERS intensity of the random horizontal nanowires was normalized to the total number of random NWs in the 2 micron area.

To explain the enhancement in the SERS intensity for the closely spaced NW arrays, we refer to Kotmann and Martin [61], who have shown that 2 parallel NWs with a small separation distances can result in the formation of hot spots corresponding to very intense electric field, leading to a significantly enhanced coupled plasmon resonance.

In order to understand the enhancement in the case of our closely spaced aligned high density nanowire arrays, we have performed COMSOL electric field calculations, shown in Fig. 10, which show the electric fields induced between the NW arrays upon irradiation by light. As can be seen in Fig. 10(a), for a 4x4 array, parallel and closely packed NWs induced high electric fields along the whole lengths of the nanowires, which may account for the very large enhancement of the observed SERS signals. Figure 10(b) is a side view of the parallel NW arrays and the electric fields generated, clearly demonstrating the strong plasmonic coupling between the NWs in the array. Due to the difficulty of computing electric fields for long NWs, only 300 nm long wires were modeled. However, these results are also applicable to longer NWs. Furthermore, COMSOL simulations also show that

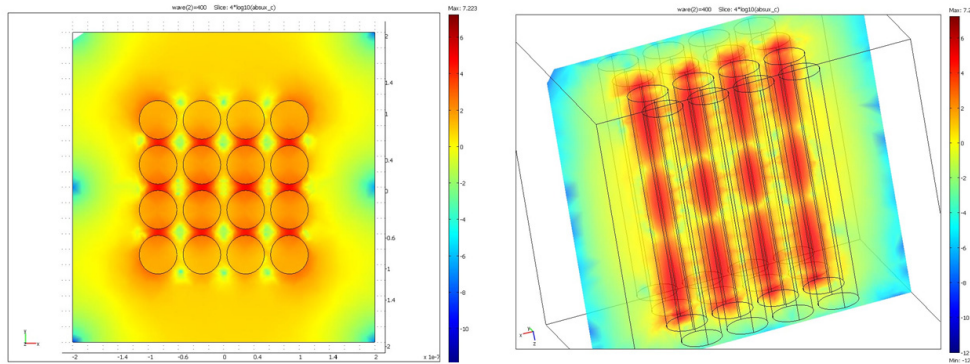


Fig. 10. COMSOL simulation of the electric field enhancement of closely spaced Ag nanowire arrays a) looking from top and b) along the NWs. In the simulations, the NWs were 100 nm in diameter and 300 nm in length.

on average, the strong plasmonic coupling is not dramatically influenced by small variations in the nanowire diameters. Since the nanowires in the arrays are aligned but randomly spaced from each other, if one assumes that some fraction of the nanowires are significantly closer than the average distance of 150-200 nm, strong plasmon coupling and thus a high SERS intensity would be expected, as discussed by Kotmann et al. [61]. The fact that these nanowires form regions where they are much more closely spaced is clearly seen in Fig. 1(b), 1(c).

## Conclusions

In summary, we have synthesized arrays of silver coated silicon nanowires and studied their properties theoretically and experimentally. The arrays, which had a thicker Ag coating, have been predicted to have a hyperbolic dispersion in the visible and infrared ranges of the spectrum, modeled by finite-element-based solutions of Maxwell's equations. In terms of experimental results, we have noted a significant reduction of the samples' reflectance at p polarization (in comparison to s polarization), which is expected from rough surfaces of a hyperbolic metamaterial. Furthermore, the emission behavior of dye molecules deposited on top of the nanowire arrays has been obtained, and the results show strong dye emission quenching, by nearly an order of magnitude, and shortening of the emission kinetics. These two observations are consistent with the theoretical predictions for hyperbolic metamaterials.

The measured SERS signals for the Si/Ag array composites were enhanced by almost an order of magnitude for closely packed and aligned nanowires, compared to random nanowire composites deposited on a flat surface. COMSOL electric field simulations suggest that this enhancement is due to plasmon coupling in closely spaced nanowires, which are present in the arrays investigated.

## Acknowledgments

The authors would like to thank Eric Epstein, Hua Qi, Alice King and Erin Cleveland for experimental assistance. The authors also thank Evgenii Narimanov for useful discussions. The authors thank the Office of Naval Research for financial support. J.E.L., T.U.T, J.K.K, G.Z, and M.A.N. acknowledge the supported by the NSF PREM grant DMR-1205457, NSF IGERT grant DGE-0966188, and AFOSR grant FA9550-09-1-0456, V.P. acknowledges support from NSF MWN grant DMR-1209761 and ARO grant W911NF-12-1-0533.